TiO₂ Nanofibrous Interface Development for Raman Detection of Environmental Pollutants

D. Maznichenko
Ryerson University

P. R. Selvaganapathy
McMaster University

K. Venkatakrishnan
Ryerson University

B. Tan
Ryerson University

TiO2 nanofibrous interface development for Raman detection of environmental pollutants

D. Maznichenko, P. R. Selvaganapathy, K. Venkatakrishnan, and B. Tan

TiO$_2$ nanofibrous interface development for Raman detection of environmental pollutants

D. Maznichenko,[1] P. R. Selvaganapathy,[2] K. Venkatakrishnan,[1] and B. Tan[3,a]

[1]*Department of Mechanical and Industrial Engineering, Ryerson University, Toronto, 350 Victoria Street, Ontario M5B 2K3, Canada*
[2]*Department of Mechanical Engineering, McMaster University, Hamilton, 1280 Main Street West, Ontario L8S 4L7, Canada*
[3]*Department of Aerospace Engineering, Ryerson University, Toronto, 350 Victoria Street, Ontario M5B 2K3, Canada*

Sensor development has been reliant on planar Au and Ag nanoparticle research. The current findings explored a unique 3-D network of crystalline TiO$_2$ nanoparticles linked as nanofibers. In addition to the favorability of using TiO$_2$ for chemical and bio-molecular sensing, the nanofiber network provides molecular diffusion control and an increased confocal volume signal. Controlled femtosecond laser synthesis is also demonstrated that directly impacts surface-enhanced Raman spectroscopy detection of two common environmentally harmful chemicals: bisphenol A and diclofenac sodium salt. These findings assert that 3-D nanofibrous network porosity optimization is crucial for Raman monitoring of drinking water. © *2012 American Institute of Physics.*
[http://dx.doi.org/10.1063/1.4769112]

Bisphenol A (BPA) is a common polycarbonate (PC) monomer. Krishnan *et al.* discovered that BPA can be released from PC products during autoclaving and then dissolve into the surrounding environment.[1] BPA is also a known endocrine disrupter which leads to a disturbed hormone balance in humans.[2] Diclofenac sodium salt (DCFNa) is a non-steroidal and anti-inflammatory pharmaceutical ingredient. However, DCFNa is also amongst the most commonly detected pharmaceutically active compounds in ground and surface water.[3] Since chemical adsorption can target human organs, it is important to have analytical capacity for molecular level identification and adsorption analysis of these aromatic compounds in environmental samples.

Raman vibrational spectroscopy has evolved into a real-time analytical tool for species characterization. It is label free, non-invasive, and unaffected by water in aqueous solutions.[4,5] Surface-enhanced Raman spectroscopy (SERS) relies mainly on unperturbed plasmonic resonance.[6] This makes various nanoparticle geometries of Au, Ag, and Au-Ag composites popular for optofluidic and chromatography SERS devices.[7–10] However, Au typically needs a surfactant for stabilization such as toxic cetyltrimethylammonium bromide (CTAB).[11] Therefore, smaller Au nanoparticles tend to be used despite worse SERS performance. Ag is several orders of magnitude more SERS active than Au,[12] but the notorious oxide layer of Ag induces fluctuations in SERS as well as Raman laser-induced structural changes.[13]

On the other hand, TiO$_2$ is thermodynamically stable,[14] attracts water and water soluble molecules,[15] favorable for bio-molecular bonding,[16] and it is corrosion resistant with a stable oxide surface.[17] Recent research shows that the femtosecond laser irradiation method can generate a unique TiO$_2$ 3-D nanofibrous network under ambient conditions with no

pre/post processing.[18] This architecture is described as a quasi-random scaffold of singly chained 15–150 nm diameter crystalline nanoparticles.

The unique 3-D nanofibrous network of quasi-organized nanoparticle clusters features additional characteristics in favor of species detection by SERS. In particular, the high dielectric damping of TiO$_2$ is alleviated by various electromagnetic phenomena of the nanofiber such as the nanogap, nanocluster, and plasmonic hybridization.[19] In addition, the network depth fully utilizes the lasers' confocal volume for detection of Stokes shifted photons. The inherent nanofibrous porosity also controls molecular diffusion which is critical in micro-spot sized optical spectroscopy techniques.[20,21] In this study, we have demonstrated controllable surface roughness and porosity which was directly related to SERS activity of BPA and DCFNa. These findings impact the SERS sensor pad development towards chemical and bio-molecular sensing applications.

A femtosecond laser with diode-pumping, mode-locking, and Yb-doped fiber amplification (Clark-MXR IMPULSETM Series) was used to generate the TiO$_2$ nanofibers from a commercially pure titanium (Ti) substrate. Synthesis control by laser repetition rate and irradiation time (i.e., dwell time) was investigated. The central laser wavelength (generated second harmonic at 515 nm), power (16 W), pulse duration (214 fs), polarization (circular), and piezo scanning speed (1000 μm/s) were kept constant under single pulse irradiation. These parameters were selected based on an earlier investigation of Ti nanofiber synthesis.[18] Prior to irradiation, a dot-array pattern was plotted with EzCAD$^{©}$ software. Once galvanometer scanning was initiated, the acousto-optical modulator blocked the irradiation between successive points. It is also readily possible to design various channels and junctions if desired.[22]

To simulate pollutant detection using Raman signals under environmental conditions, drinking water was used as a solvent for BPA and DCFNa. Drinking water analysis

---
a)Author to whom correspondence should be addressed. Electronic mail: tanbo@ryerson.ca.

revealed that Na, Ca, Cl, and Cl$^-$ are the most concentrated inorganic materials. SERS contributing elements were also studied but were found to be relatively negligible (Table S1 in supplementary material[43]).

Dried residue and aqueous solutions of DCFNa and BPA were investigated under Raman spectroscopy. The aqueous solutions were prepared with 0.5 mM pollutant concentration in drinking water and applied immediately prior to Raman spectroscopy measurements. For dry residue studies, the sensor pads were dried on a hotplate at 60 °C. Both BPA and DCFNa are thermally stable at 60 °C.[23] Each particular experimental condition was repeated on average 5–7 times across different sites for a particular sensor pad hence space averaging the results.

The laser excitation wavelength for Raman spectroscopy was 532 nm. The equipment lower wavenumber limit was 150 cm^{-1}. DCFNa and BPA spectra beyond 1650 cm^{-1} are lower intensity summation bands representing a minority of characteristic vibrational modes.[24] Data acquisition parameters were chosen based on trial-and-error for repeatable spectra results with minimum noise. The exposure time was 7 s with a five time repetition. A D2 filter (reducing power to 1 mW) with a 50× objective was used. No laser heating effect is expected under such conditions.[25,26] No reporter molecules were used.

Low scanning speed AFM in contact mode was used to penetrate the nanofibers and reveal the surface morphology. SEM was used to qualify the 3-D network porosity changes and general sensor pad morphology. Scanning near-field microscopy (SNOM) at 514 nm with an aluminum coated fiber probe (nominal aperture 100 nm) was used to study the optical behavior of individual micro-vias. A quartz tuning fork at resonance frequency was used for scanning probe feedback on sample approach. Additional experimental details are presented in supplementary material (S1).[43]

Fig. 1 demonstrates the synthesis control of the TiO$_2$ nanofibrous 3-D network by using the pulsed femtosecond laser. The nanofiber network depth, 3-D clustering (i.e., average porosity), sensor pad surface morphology, as well as the nanoparticle size and variation have various degrees of independent controllability.[18] For example, increasing the irradiation dwell time increases the network depth while reducing porosity. It is also important to have a nanofiber particle size distribution. The larger nanoparticles are known to promote solute adsorption while SERS stabilization is achieved by the smaller nanoparticles.[27] Both the laser repetition rate and the irradiation time affect the nanofiber particle population. Micro-via effects on Raman spectroscopy have been included with supporting information.

In addition, the Raman spectrum inset of Fig. 1 shows that it is possible to have a dominantly rutile or a mixture of rutile and anatase TiO$_2$ phases. Anatase forms at higher laser dwell time but more predominantly with higher pulse energy (especially below the 13 MHz laser repetition rate). TiO$_2$ conforms to D$_{4h}$ symmetry with rutile modes detected as B_{1g} (144), E_g (443), A_{1g} (611), and B_{2g} (825) cm^{-1}.[28] Anatase modes appear as E_g' (144), E_g'' (197), B_{1g}' (400), B_{1g}'' (515), A_{1g} (519), and E_g (640) cm^{-1}.[29] TiO$_2$ peak shifting was minimal between the studied sensor pads and was likely affected by relative TiO$_2$ phase mixtures.
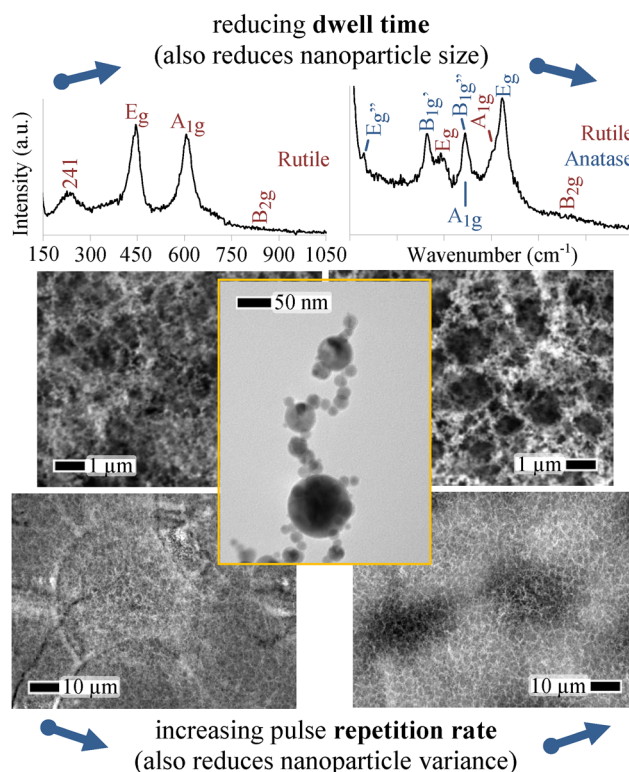

FIG. 1. Summarized synthesis controllability of the TiO$_2$ 3-D nanofibrous sensor pad; Raman spectra (top), SEM (sides), TEM (centre).

Background noise dominates the Raman spectra with a commercial Ti substrate (Fig. S1). However, the TiO$_2$ nanofibrous sensor pads exhibit appreciable BPA detection improvement under aqueous conditions (Fig. 2). BPA conforms to C$_{2h}$ symmetry with 72 irreducible vibration modes.[30] BPA features two hydroxyl groups that could potentially compete against dissociated water, especially on rutile TiO$_2$.[31] However, there was no enhancement of BPA dry residue across all studied sensor pads. The BPA SERS spectra under aqueous conditions will be briefly commented on here.

It is possible for additional modes and peak shifting to dominate the Raman spectra under SERS.[32] In Fig. 2, the BPA C-H bending modes (700–1000 cm^{-1}) have been significantly affected. Strong modes also appear at 1536, 1570, 1581, and 1610 cm^{-1}, where 1581 cm^{-1} is attributed to the
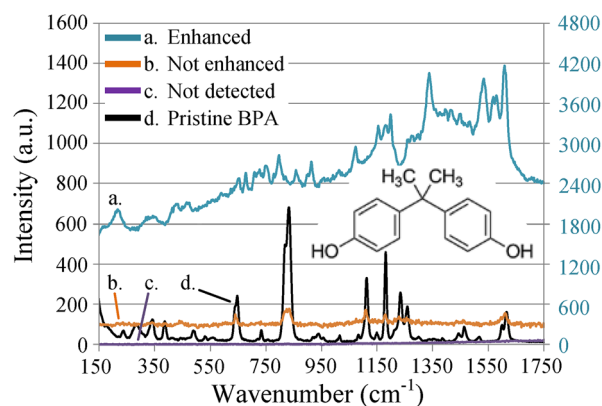

FIG. 2. Detection of aqueous (aq.) and dry residue (dr.) BPA by various sensor pads (MHz–ms): a. 4–1 (aq.), b. 13–20 (dr.), c. commercial Ti (aq. or dr.).

in-plane ring deformation and C-H bending. Such behavior from A_g and B_g modes may indicate molecular symmetry reduction by close proximity or adsorption to the surface.[6] In this case, Liu *et al.* have related a higher heat of atomization energy in metals to a stronger surface adsorption of an aromatic molecule. The Raman spectra was shown to be preserved with Ag, but can be expected to change with TiO_2 which has a heat of atomization nearly five times greater.[33,34] Other factors affecting the BPA Raman spectrum in drinking water have been considered (supplementary material (S2)[43]). At the same time, fluorescence is also evident by the high intensity Raman baseline. Since strong BPA adsorption is expected, fluorescence is attributed to a reduction in nanoparticle size.[21]

As opposed to BPA, DCFNa was detected better under dry residue conditions given its high solubility under aqueous conditions. DCFNa structure can have two nonsymmetrical isomers with 58 irreducible vibration modes. It bonds with the lone pair oxygen electrons of the carboxylate group.[35] The band at $1575 \, cm^{-1}$ shifted to $1585 \, cm^{-1}$ indicating carboxylate orientation to water even after drying.[36] However, the stable $1408 \, cm^{-1}$ band indicated that there was no dissociation of sodium. This was an expected result as drinking water already contained up to 29.6 mg/l of Na and 39.9 mg/l of Cl^- content which may substantially reduce DCFNa solubility.[37]

Fig. 3 demonstrates a gradual improvement in spectra between three selected TiO_2 sensor pads. The TiO_2 Raman background signal is clearly noticeable with sensor pads b. and c., whereas their intensity is quenched with sensor pad a. as the overall spectra improves. Such phenomenon may be indicative of improved bonding from no adsorption, to physisorption to chemisorption.[33] Optimum sensor pad parameters vary for BPA and DCFNa under aqueous and dry residue conditions and will be discussed next.

We have previously determined that for the femtosecond laser synthesis technique, the minimum TiO_2 nanonetwork generation threshold is 2 MHz (i.e., 500 ns pulse interval) at 1 ms dwell time. It was found that while a shorter pulse interval promotes a more stable plasma plume, longer dwell times promote 3-D network structuring.[18] These guidelines were
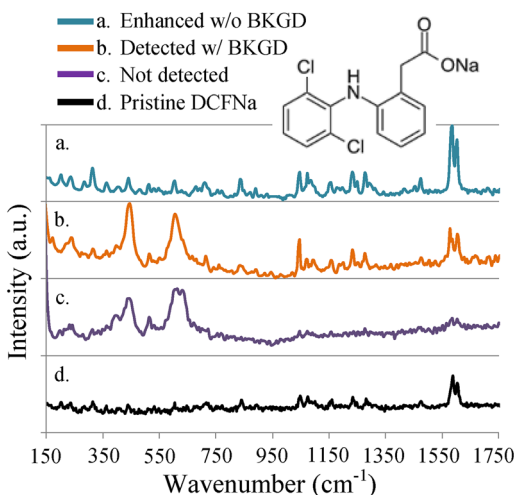
adopted for TiO_2 sensor pad development, the results of which are presented by Fig. 4. The relative sensor pad performance was ranked based on the strong carboxylic band at $1585 \, cm^{-1}$ for DCFNa and the in-plane ring stretch band at $1610 \, cm^{-1}$ for BPA.

There are two major features across all experiments as most clearly defined by the AVG sensitivity map (Fig. 4). Feature 1 is localized at longer fs pulse intervals for short 1 ms duration. These synthesis parameters were found to be preferential for the detection of both BPA and DCFNa. At the same time, the relative standard deviation is high as shown by the large diameter circles of the STDV map. These observations suggest that Feature 1 has a relatively good but also unstable performance. It is expected that aqueous conditions[9] and the micro-via morphology (Fig. S2) can contribute to STDV map variations. Since the space averaging procedure in these trials would reduce the aqueous condition variability, only the nanofiber network and the micro-via morphological contributions will be discussed further.

To begin with, the sensor pads exhibit variable hydrophilic properties. Feature 1 exhibits the most effective surface wetting.[38] Second, laser synthesis fluence is the highest at Feature 1 (Fig. S7). The corresponding change in laser plume temperature and pressure increase the anatase TiO_2 nanofiber constituency. Third, increasing the network depth (i.e., longer dwell time) with less stable plume behavior (i.e., longer pulse intervals) tends to result in null detection capacity across BPA and DCFNa experiments. Therefore, Feature 1 represents a shallow 3-D network with a high anatase to rutile ratio that is highly influenced by surface wetting.
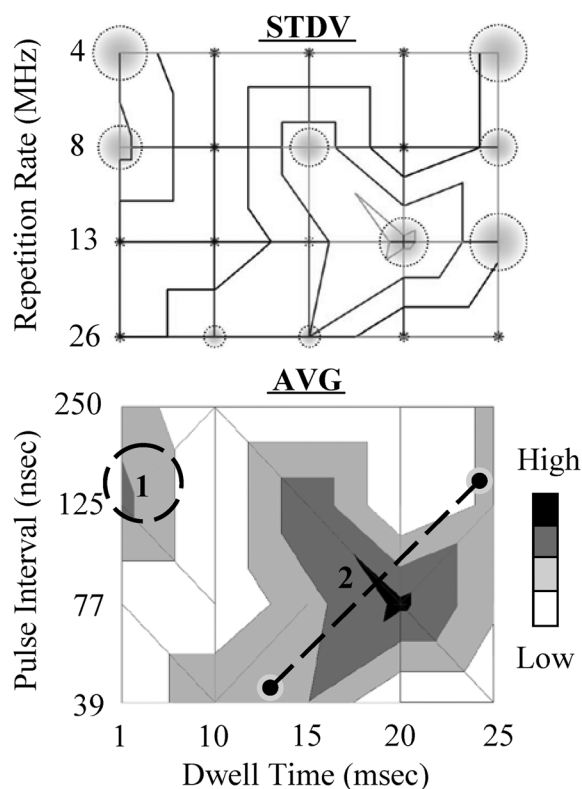
FIG. 4. Raman detection sensitivity map averaged for all TiO_2 sensor pad experiments (bottom, sensitivity increasing with color darkness) and standard deviation (top, increasing with circle diameter); pulse interval = 1/repetition rate.

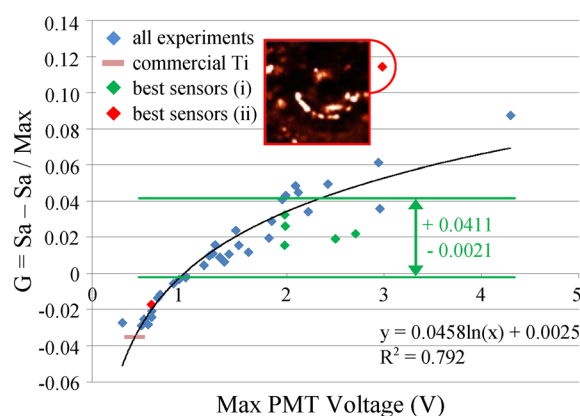FIG. 3. Detection of dry residue DCFNa by various sensor pads (MHz–ms): a. 8–15, b. 26–15, c. 4–25; note: each spectra spans ca. 200 a.u.

FIG. 5. Roughness parameter G vs. Max intensity, inset: SNOM micro-via $100 \times 100 \, \mu$m scan.

Feature 2 spans a greater Raman detection band. In general, the standard deviation reduces with a lower network depth (i.e., shorter dwell time) and with more stable plume behavior (i.e., shorter pulse intervals). However, the laser fluence at 1 ms for 39 and 77 ns pulse intervals is enough to oxidize the Ti surface but not to generate the nanofibrous 3-D networks. Moreover, porosity controls the diffusion of analytes in the 3-D nanonetwork and influences the number of metal to analyte contacts.[39] Panarin *et al.* have previously hypothesized an optimum Ag-Si substrate porosity for SERS.[40] In this case, the TiO_2 nanofibrous porosity is related by a linear combination of dwell time and pulse interval parameters which in turn influence sensor performance. Consequently, Feature 2 characterizes a field of 3-D nanofibrous networks which playoff between detection sensitivity and stability.

SNOM reflection studies were carried out to further understand the effect of sensor pad morphology and plasmon coupling. A normalized roughness construct was developed as $G = Sa - Sa/Max$, where Sa (V) is the average roughness and Max (V) is the maximum roughness (supplementary material (S3)[43]). The $G = -0.0021$ to $+0.0411$ criteria corresponds to functioning sensor pads of Fig. 4 (i.e., non-zero AVG sensitivity). Fig. 5 reveals that commercial Ti has the most uniform reflection. The next smoothest substrate was generated at 2 MHz–25 ms ($G = -0.0286$). Neither are within the G criteria and neither proved Raman detection capability. The best sensors (i) were 8–1, 8–15, 13–15, 13–20, and 26–10 (MHz–ms). Falling outside the G criteria, the best sensors (ii) were 4–25 and 26–15 (MHz–ms). Out of best sensors (ii), it is surprising that 26–15 (inset of Fig. 5) did not fall within the G criteria as its performance was moderately high with a low standard deviation (Fig. 4). Since the SNOM experiments were performed only once, at this point the aberrant G values of best sensors (ii) are attributed to experimental uncertainty such as SNOM probe damage.

Morphological information was also collected with SNOM, such as the circular micro-via ridges of Fig. S3. This information validates previous apatite precipitation observations where the lower G values relate to a higher TiO_2 surface uniformity.[38] Since the SNOM scanning feedback time is controller limited, it was not effective on such rough nanofibrous surfaces and hence it was deactivated. As a result,

both the morphology and plasmon coupling effects were present in the scans.[41]

The nanofibrous network plasmon coupling is analogous to Fibonacci array behavior. Fibonacci arrays have a quasi-periodic order (resembling Fig. 1 SEM scans). When compared to square nanoparticle arrays, the absence of periodicity prevents extended plasmon state formation allowing for larger field enhancement.[42] This phenomenon is demonstrated by localized hot-spot regions of the nanofibrous network (inset of Fig. 5). Overall, the G construct reveals that the TiO_2 nanofibrous network needs to have an optimum porosity to be Raman active. The significance of this finding establishes that nanofibrous studies with other materials cannot be dismissed as Raman inactive without porosity investigations.

In this research, a pulsed femtosecond laser was used to synthesize the unique 3-D network of crystalline TiO_2 nanofibers. Raman detection of aromatic BPA and DCFNa in drinking water was found to be sensitive with variations in network depth, surface morphological uniformity, and sensor porosity. A generalized detection map was developed which showed a strong favorability towards uniform and porous TiO_2 nanofibrous 3-D networks. In addition to making the chemical and physical favorability of TiO_2 viable for Raman spectroscopy, we have developed a unique nanoarchitecture for chemical sensing and bio-molecular detection. At the same time, the presence of hot-spots demonstrates the need for scan averaged Raman spectra collection towards commercial development of a TiO_2 based environmental sensor.

[1]A. V. Krishnan, P. Stathis, S. F. Permuth, L. Tokes, and D. Feldman, Endocrinology **132**, 2279 (1993).
[2]S. Ye, S. Morita, G. Li, H. Noda, M. Tanaka, K. Uosaki, and M. Osawa, Macromolecules **36**, 5694 (2003).
[3]A. Deng, M. Himmelsbach, Q.-Z. Zhu, S. Frey, M. Sengl, W. Buchberger, R. Niessner, and D. Knopp, Environ. Sci. Technol. **37**, 3422 (2003).
[4]Z. Xu, M. R. Gartia, C. J. Choi, J. Jiang, Y. Chen, B. T. Cunningham, and G. L. Liu, J. Raman Spectrosc. **42**, 1939 (2011).
[5]X. Zhang, M. A. Young, O. Lyandres, and R. P. Van Duyne, J. Am. Chem. Soc. **127**, 4484 (2005).
[6]J. R. Lombardi and R. L. Birke, J. Phys. Chem. C **112**, 5605 (2008).
[7]Z. Wang, S. Zong, J. Yang, C. Song, J. Li, and Y. Cui, Biosens. Bioelectron. **26**, 241 (2010).
[8]L. Tong, M. Righini, M. U. Gonzalez, R. Quidant, and M. Käll, Lab Chip **9**, 193 (2009).
[9]Y. S. Huh and D. Erickson, Biosens. Bioelectron. **25**, 1240 (2010).
[10]D. Li, L. Qu, W. Zhai, J. Xue, J. S. Fossey, and Y. Long, Environ. Sci. Technol. **45**, 4046 (2011).
[11]A. M. Alkilany, P. K. Nagaria, C. R. Hexel, T. J. Shaw, C. J. Murphy, and M. D. Wyatt, Small **5**, 701 (2009).
[12]S. Lee, S. Kim, J. Choo, S. Y. Shin, Y. H. Lee, H. Y. Choi, S. Ha, K. Kang, and C. H. Oh, Anal. Chem. **79**, 916 (2007).
[13]D. Büchel, C. Mihalcea, T. Fukaya, N. Atoda, J. Tominaga, T. Kikukawa, and H. Fuji, Appl. Phys. Lett. **79**, 620 (2001).
[14]A. Vittadini, A. Selloni, F. P. Rotzinger, and M. Grätzel, Phys. Rev. Lett. **81**, 2954 (1998).
[15]J. E. Ellingsen, Biomaterials **12**, 593 (1991).
[16]B. Li, R. Franking, E. C. Landis, H. Kim, and R. J. Hamers, ACS Appl. Mater. Interfaces **1**, 1013 (2009).
[17]T. Albrektsson, P. I. Branemark, H. A. Hansson, and J. Lindstrom, Acta Orthop. Scand. **52**, 155 (1981).
[18]M. Sivakumar, K. Venkatakrishnan, and B. Tan, Nanotechnology **21**, 225601 (2010).

[19]Z. Tian, Z. Yang, and D. Wu, *SERS from Transition Metals and Excited by Ultraviolet Light* (Springer, 2006), Chap. 7.

[20]H. C. Yoon and H.-S. Kim, Anal. Chem. **72**, 922 (2000).

[21]C. L. Haynes, A. D. McFarland, and R. P. Van Duyne, Anal. Chem. **77**, 338A (2005).

[22]S. Jariwala, K. Venkatakrishnan, and B. Tan, Opt. Express **18**, 1630 (2010).

[23]M. K. Nazeeruddin, A. Kay, I. Rodicio, R. Humphry-Baker, E. Muller, P. Liska, N. Vlachopoulos, and M. J. Gratzel, J. Am. Chem. Soc. **115**, 6382 (1993).

[24]M. A. Gauthier, I. Stangel, T. H. Ellis, and X. X. Zhu, Biomaterials **26**, 6440 (2005).

[25]R. C. Maher, J. Hou, L. F. Cohen, E. C. Le Ru, J. M. Hadfield, J. E. Harvey, P. G. Etchegoin, F. M. Liu, M. C. Green, and R. J. C. Brown, J. Chem. Phys. **123**, 084702 (2005).

[26]S. Sahoo, A. K. Arora, and V. Sridharan, J. Phys. Chem. C **113**, 16927 (2009).

[27]P. Tarakeshwar, D. Finkelstein-Shapiro, S. J. Hurst, T. Rajh, and V. Mujica, J. Phys. Chem. C **115**, 8994 (2011).

[28]S. P. S. Porto, P. A. Fleury, and T. C. Damen, Phys. Rev. **154**, 522 (1967).

[29]T. Ohsaka, F. Izumi, and Y. Fujiki, J. Raman Spectrosc. **7**, 321 (1978).

[30]M. Kurt and S. Yurdakul, J. Mol. Struct. **654**, 1 (2003).

[31]G. Li, S. Morita, S. Ye, M. Tanaka, and M. Osawa, Anal. Chem. **76**, 788 (2004).

[32]M. V. Canamares, C. Chenal, R. L. Birke, and J. R. Lombardi, J. Phys. Chem. C **112**, 20295 (2008).

[33]G.-K. Liu, B. Ren, D.-Y. Wu, S. Duan, J.-F. Li, J.-L. Yao, R.-A. Gu, and Z.-Q. Tian, J. Phys. Chem. B **110**, 17498 (2006).

[34]K. S. Jeong, C. Chang, E. Sedlmayr, and D. Sulzle, J. Phys. B **33**, 3417 (2000).

[35]T. Iliescu, M. Baia, and W. Kiefer, Chem. Phys. **298**, 167 (2004).

[36]Van Der J. Weerd and S. Kazarian, J. Pharm. Sci. **94**, 2096 (2005).

[37]M.-T. Sheu, H.-L. Chou, C.-C. Kao, C.-H. Liu, and T. D. Sokoloski, Int. J. Pharm. **85**, 57 (1992).

[38]A. Tavangar, B. Tan, and K. Venkatakrishnan, Acta Biomater. **7**, 2726 (2011).

[39]M. Baia, G. Melinte, L. Barbu-Tudoran, L. Diamandescu, V. Iancu, V. Cosoveanu, V. Danciu, and L. Baia, J. Phys.: Conf. Ser. **304**, 012059 (2011).

[40]A. Yu Panarin, S. N. Terekhov, K. I. Kholostov, and V. P. Bondarenko, Appl. Surf. Sci. **256**, 6969 (2010).

[41]G. Wurtz, J. Hranisavljevic, and G. Wiederrecht, Nano Lett. **3**, 1511 (2003).

[42]R. Dallapiccola, A. Gopinath, F. Stellacci, and L. Negro, Opt. Express **16**, 5544 (2008).

[43]See supplementary material at http://dx.doi.org/10.1063/1.4769112 for acquiring Raman and SNOM data (S1), BPA SERS spectrum analysis (S2), and determining the best Raman sensor pad (S3).